An Hermitian finite element solution of the two-dimensional saturated-unsaturated flow equation

M. Th. VAN GENUCHTEN

US Salinity Laboratory, 4500 Glenwood Drive, Riverside, California 92501, USA

This paper describes a Galerkin-type finite element solution of the two-dimensional saturated-unsaturated flow equation. The numerical solution uses an incomplete (reduced) set of Hermitian cubic basis functions and is formulated in terms of normal and tangential coordinates. The formulation leads to continuous pressure gradients across interelement boundaries for a number of well-defined element configurations, such as for rectangular and circular elements. Other elements generally lead to discontinuous gradients; however, the gradients remain uniquely defined at the nodes. The method avoids calculation of second-order derivatives, yet retains many of the advantages associated with Hermitian elements. A nine-point Lobatto-type integration scheme is used to evaluate all local element integrals. This alternative scheme produces about the same accuracy as the usual 9- or 16-point Gaussian quadrature schemes, but is computationally more efficient.

INTRODUCTION

The frequent use of land for the disposal of a wide variety of industrial, municipal and agricultural wastes emphasizes the need for an accurate quantitative description of flow and transport in the unsaturated zone. Initially, mostly finite difference methods were used to solve the governing flow equations.[1-4] Finite element techniques became available in the late 1960s and have since been applied to two-dimensional saturated-unsaturated flow problems by Neuman,[5] Reeves and Duguid,[6] Segol,[7] and many others. The finite element solution presented here uses first-order continuous Hermitian cubic basis functions. If properly applied, this method generates continuous pressure head gradients across interelement boundaries, and hence produces a continuous flow velocity field over the entire domain. Earlier work dealing with one-dimensional flow and transport showed that the Hermitian approach generated better results than was possible with either standard finite differences or linear finite elements, particularly with respect to the material balance for the transport equation.[8] This study is limited to solutions of the flow equation only.

GOVERNING FLOW EQUATION

The governing equation for transient saturated-unsaturated flow in a two-dimensional vertical cross-section is taken as

$$L(h) \equiv \frac{\partial}{\partial x_\alpha}\left(K_{\alpha\beta}\frac{\partial h}{\partial x_\beta} + K_{\alpha\beta}\right) - C\frac{\partial h}{\partial t} + Q = 0 \quad (\alpha, \beta = 1, 2) \tag{1}$$

where L is a differential operator, h is the pressure head, $K_{\alpha\beta}$ is the hydraulic conductivity, Q is a fluid source, t is the time and x_α is the α-th spatial coordinate. The soil water capacity C is

$$C = \left(\frac{\theta}{\epsilon}S + \epsilon\frac{\partial S_w}{\partial h}\right) \tag{2}$$

where θ is the volumetric soil water content, S is the specific storage coefficient, S_w is the degree of fluid saturation and ϵ is the porosity.

GALERKIN APPROXIMATION

Equation (1) will be solved with the Galerkin-type finite element method. The dependent variable h is assumed to be of the form

$$h(x_\alpha, t) \simeq \sum_{j=1}^{n} \phi_j(x_\alpha)\, a_j(t) \tag{3}$$

where the ϕ_j are the selected basis functions and where the a_j are the associated time-dependent coefficients. The basis functions are used also to minimize the residual $L(h)$ of equation (1) by requiring that

$$\int_\Omega L\,[h(x_\alpha, t)]\;\phi_i(x_\alpha)\,\mathrm{d}\Omega = 0 \tag{4}$$

where Ω represents the two-dimensional domain. Combining equations (1), (3) and (4), and applying Green's first theorem to the spatial derivatives leads to

$$[\mathbf{P}]\{\mathbf{X}\} + [\mathbf{R}]\frac{\mathrm{d}\{\mathbf{X}\}}{\mathrm{d}t} + \{\mathbf{F}\} = 0 \tag{5}$$

where

$$\{\mathbf{X}_j\} = \{\mathbf{a}_j\} \tag{6a}$$

Presented at the Fourth International Conference on Finite Elements in Water Resources, Inst. f. Stromungsmechanik, University of Hannover, Fed. Rep. of Germany, 21-25 June 1982.

Received July 1982. Written discussion closes August 1983.

0309-1708/83/020107-06$2.00

$$[\mathbf{P}_{ij}] = \int_\Omega K_{\alpha\beta} \frac{\partial \phi_j}{\partial x_\beta} \frac{\partial \phi_i}{\partial x_\alpha} \, d\Omega \tag{6b}$$

$$[\mathbf{R}_{ij}] = \int_\Omega C \phi_j \phi_i \, d\Omega \tag{6c}$$

$$\{\mathbf{F}_i\} = \int_\Omega \left(-Q\phi_i + K_{\alpha 2} \frac{\partial \phi_i}{\partial x_\alpha} \right) d\Omega + \int_\Gamma q_n \phi_i \, d\Gamma \tag{6d}$$

in which Γ represents the boundary of Ω. The parameter q_n in equation (6d) holds for applied flux-type boundary conditions:

$$q_n(x_\alpha, t) = -\left(K_{\alpha\beta} \frac{\partial h}{\partial x_\alpha} + K_{\alpha 2} \right) n_\alpha \tag{7}$$

where n_α is the outward normal to the boundary Γ.

Basis functions

When equation (3) is applied to a one-dimensional element (x_a, x_b) and first-order continuous Hermitian basis functions are used, its form reduces to

$$h(\xi, t) = \sum_{j=1}^{2} \left\{ \phi_{0j}(\xi) H_j(t) + \phi_{1j}(\xi) \frac{dH_j(t)}{d\xi} \right\} \tag{8}$$

The local coordinate ξ in equation (8) is related to the global x-coordinate through the expression

$$\xi = -1 + \frac{2}{\Delta x}(x - x_a) \tag{9}$$

where $\Delta x = x_b - x_a$ is the nodal distance of the element. The one-dimensional Hermitian cubic basis functions are

$$\phi_{0j} = -\tfrac{1}{4}(\xi + \xi_0)^2 (\xi\xi_0 - 2) \qquad (\xi_0 = \pm 1) \tag{10a}$$

$$\phi_{1j} = \tfrac{1}{4}\xi_0(\xi + \xi_0)^2 (\xi\xi_0 - 1) \qquad (\xi_0 = \pm 1) \tag{10b}$$

As is the case with zero-order continuous basis functions, the two-dimensional Hermitian basis functions can be generated from the one-dimensional expressions in at least two ways. In one approach, the two-dimensional functions are obtained by simply multiplying the one-dimensional expressions with each other. This approach leads to four unknowns per node: the function H, its spatial derivatives $\partial H/\partial x$ and $\partial H/\partial z$, and the cross-derivative $\partial^2 H/\partial x \, \partial z$, where $x = x_1$ and $z = x_2$ are the global coordinates. Unfortunately, this approach also leads to the derivatives $\partial^2 H/\partial x^2$ and $\partial^2 H/\partial z^2$ in the global matrix equation when applied to deformed non-rectangular elements. These higher order derivatives must be retained in the formulation if first-order continuity in the pressure head across inter-element boundaries is required. When the higher order derivatives are neglected, the gradients still will be continuous at the nodes, but generally not across element boundaries between nodes.

An alternative approach would be to eliminate the cross-derivative from the formulation altogether, thus avoiding the calculation of unnecessary quantities and reducing the number of unknowns per node from four to three. This approach leads to the following expansion for the unknown function over the local element of Fig. 1:[9]

$$h(\xi, \eta, t) = \sum_{j=1}^{4} \left(\phi_{00j} H_j + \phi_{10j} \frac{\partial H_j}{\partial \xi} + \phi_{01j} \frac{\partial H_j}{\partial \eta} \right) \tag{11}$$

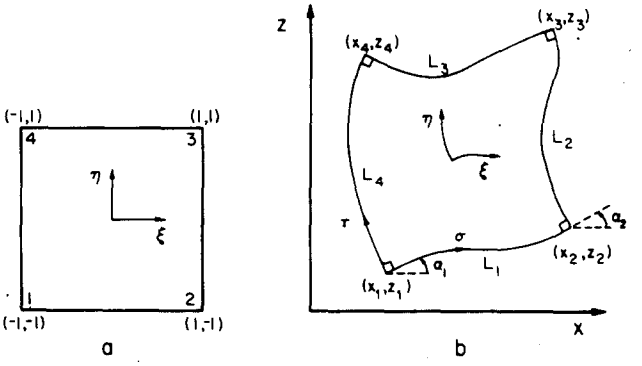

Figure 1. Deformed isoparametric Hermitian elements in local (a) and global (b) coordinates

where the basis functions ϕ are given by

$$\phi_{00j} = \tfrac{1}{8}(1 + \xi\xi_0)(1 + \eta\eta_0)(2 + \xi\xi_0 + \eta\eta_0 - \xi^2 - \eta^2) \tag{12a}$$

$$\phi_{10j} = -\tfrac{1}{8}\xi_0(1 + \xi\xi_0)(1 + \eta\eta_0)(1 - \xi^2) \tag{12b}$$

$$\phi_{01j} = -\tfrac{1}{8}\eta_0(1 + \xi\xi_0)(1 + \eta\eta_0)(1 - \eta^2) \tag{12c}$$

in which $\xi_0 = \pm 1$ and $\eta_0 \pm 1$.

Normal and tangential coordinates

The finite element scheme presented here is formulated in terms of normal and tangential coordinates (σ, τ; see Fig. 1b). The advantage of this method is that flux-type boundary conditions are much easier to incorporate into the numerical scheme. In addition, the study is restricted to deformed elements that have 90° internal angles. This restriction could limit in some cases the applicability of the solution, particularly when highly irregular boundaries are present.[11] However, because most field problems can be described easily with elements having 90° angles, and because the formulation could be simplified, it was felt advantageous to maintain the square angles. A different formulation is needed for those few cases where this restriction cannot be met.

When normal and tangential coordinates are used, the unknown nodal coefficients become H and its derivatives $\partial H/\partial\sigma$ and $\partial H/\partial\tau$. Hence, approximation (11) must be rewritten in terms of these unknowns. From the chain rule of differentiation we have

$$\frac{\partial H_j}{\partial \xi} = \frac{\partial H_j}{\partial \sigma}\frac{\partial \sigma_j}{\partial \xi} + \frac{\partial H_j}{\partial \tau}\frac{\partial \tau_j}{\partial \xi} \tag{13a}$$

$$\frac{\partial H_j}{\partial \eta} = \frac{\partial H_j}{\partial \sigma}\frac{\partial \sigma_j}{\partial \eta} + \frac{\partial H_j}{\partial \tau}\frac{\partial \tau_j}{\partial \eta} \tag{13b}$$

Because the distorted elements have 90° internal angles, it follows immediately that all derivatives $\partial\tau/\partial\xi$ and $\partial\sigma/\partial\eta$ are zero. The other nodal derivatives in equation (13) can be expressed in terms of the geometric properties of the element. For example, for node 1 of the deformed element in Fig. 1b we have

$$\frac{\partial \sigma_1}{\partial \xi} = \frac{L_1}{2} \qquad \frac{\partial \tau_1}{\partial \eta} = \frac{L_4}{2} \tag{14}$$

where L_1 and L_4 are the lengths of element sides 1 and 4, respectively. Substituting equation (13) into equation (11) and using the information above yields

$$h(\xi, \eta, t) = \sum_{j=1}^{4} \left(\phi_{00j} H_j + \phi_{\sigma j} \frac{\partial H_j}{\partial \sigma} + \phi_{\tau j} \frac{\partial H_j}{\partial \tau} \right) \tag{15}$$

with the new basis functions

$$\phi_{\sigma j} = \phi_{10j} \frac{\partial \sigma_j}{\partial \xi} \qquad \phi_{\tau j} = \phi_{01j} \frac{\partial \tau_j}{\partial \eta} \tag{16}$$

The following isoparametric transformation is used for distorted elements:[11]

$$x(\xi, \eta) = \sum_{j=1}^{4} \left(\phi_{00j} X_j + \phi_{\sigma j} \frac{\partial X_j}{\partial \sigma} + \phi_{\tau j} \frac{\partial X_j}{\partial \tau} \right) \tag{17a}$$

$$z(\xi, \eta) = \sum_{j=1}^{4} \left(\phi_{00j} Z_j + \phi_{\sigma j} \frac{\partial Z_j}{\partial \sigma} + \phi_{\tau j} \frac{\partial Z_j}{\partial \tau} \right) \tag{17b}$$

where the coefficients represent the nodal values of the x and z coordinates and their normal and tangential derivatives:

$$\frac{\partial X_j}{\partial \sigma} = \cos(\alpha_j) \qquad \frac{\partial Z_j}{\partial \sigma} = \sin(\alpha_j) \tag{18a}$$

$$\frac{\partial X_j}{\partial \tau} = -\sin(\alpha_j) \qquad \frac{\partial Z_j}{\partial \tau} = \cos(\alpha_j) \tag{18b}$$

Finally, the side lengths L_i in equation (14) can be obtained by numerically integrating equations of the form:[9]

$$L = \int_{-1}^{1} \left\{ \left(\frac{\partial x}{\partial \xi} \right)^2 + \left(\frac{\partial z}{\partial \xi} \right)^2 \right\}^{1/2} d\xi \qquad (\eta, \eta_0 = \pm 1) \tag{19}$$

Numerical integration

Numerical techniques are used to evaluate the integrals in equation (6). The integrations are carried out directly on the local (ξ, η) element between the limits -1 and $+1$. For this purpose, the area elements $d\Omega$ in equation (6) are replaced by

$$d\Omega = \det(J)\, d\xi\, d\eta \tag{20}$$

where J is the Jacobian of the transformation. Several methods are available to carry out the numerical integrations over each local element. Typically, an integral is approximated by a sum consisting of the values of the function at selected points in the local element and multiplied by appropriate weighting coefficients. For example, for the function $f(\xi, \eta)$ we have

$$\int_{-1}^{1} \int_{-1}^{1} f(\xi, \eta)\, d\xi\, d\eta = \sum_{k=1}^{n} w_k f(\xi_k, \eta_k) + E \tag{21}$$

where (ξ_k, η_k) are the coordinates of the integration point, w_k is the associated weighting coefficient, and E is the error of the approximation. Gaussian quadrature schemes have been used nearly without exception in related finite element studies. Although Gaussian quadrature probably is the most accurate scheme for a given number of integration points, this approach does not take full advantage of the properties of Hermitian basis functions. These basis functions, including their derivatives, are zero on several or all corner nodes. Hence, the computational effort can be reduced by locating some of the integration points at the nodes. Consequently, an alternative nine-point Lobatto-type quadrature scheme was used for all numerical integrations. Figure 2 shows the location of the nine integration points: four at the nodes and five inside the element. The integration error E for this scheme is slightly less than the error for 3 x 3 Gaussian quadrature.[10]

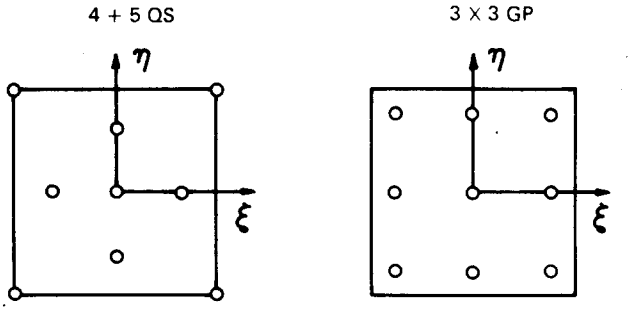

ξ_k	η_k	w_k
± 1	± 1	1/9
$\pm\sqrt{0.4}$	0	10/9
0	$\pm\sqrt{0.4}$	10/9
0	0	−8/9

ξ_k	η_k	w_k
$\pm\sqrt{0.6}$	$\pm\sqrt{0.6}$	25/81
0	$\pm\sqrt{0.6}$	40/81
$\pm\sqrt{0.6}$	0	40/81
0	0	64/81

Figure 2. Location of integration points and values of weighting coefficients for the nine-point Lobatto-type (4 + 5 QS) and nine-point Gaussian quadrature (3 x 3 GP) schemes

Integration in time

Equation (5) defines a set of n ordinary differential equations in n unknowns. A finite difference scheme was introduced to approximate the time derivative in the matrix equation. Define for that purpose:

$$\left\{ \frac{d\mathbf{X}}{dt} \right\}^{t+\Delta t/2} \simeq \frac{\{\mathbf{X}\}^{t+\Delta t} - \{\mathbf{X}\}^{t}}{\Delta t} \tag{22a}$$

$$\{\mathbf{X}\}^{t+\Delta t/2} \simeq \omega \{\mathbf{X}\}^{t+\Delta t} + (1-\omega)\{\mathbf{X}\}^{t} \tag{22b}$$

where Δt is the time step and ω a temporal weighting coefficient ($0 \leqslant \omega \leqslant 1$). Defining matrix equation (5) at the half-time level and substituting equations (22a, b) into equation (5) leads to the following set of equations:

$$[\mathbf{A}]^{t+\Delta t/2} \{\mathbf{X}\}^{t+\Delta t} = [\mathbf{B}]^{t+\Delta t/2} \{\mathbf{X}\}^{t} + \{\mathbf{F}\}^{t+\Delta t/2} \tag{23}$$

where

$$[\mathbf{A}] = \omega[\mathbf{P}] + \frac{1}{\Delta t}[\mathbf{R}] \tag{24a}$$

$$[\mathbf{B}] = (\omega - 1)[\mathbf{P}] + \frac{1}{\Delta t}[\mathbf{R}] \tag{24b}$$

The iterative scheme used to solve equation (23) was exactly the same as the scheme employed earlier for similar one-dimensional flow situations.[8]

Boundary conditions

Constant pressure head (Dirichlet-type) boundary conditions were included in two ways. First, all algebraic equations that are associated with constant boundary nodes were eliminated from matrix equation (23). Second, Dirichlet boundary conditions also affect those line integrals of equation (6d) that are associated with the normal and tangential gradients of the pressure head. To calculate these terms, one must first evaluate the flux q_n normal to the boundary. This procedure leads to equivalent nodal values for the line integrals; these nodal values must be added to the vector $\{\mathbf{F}\}$.[11]

A similar approach applies also to flux-type boundary conditions. When the pressure gradient or the flux normal to a boundary is specified, either $\partial H/\partial\sigma$ or $\partial H/\partial\tau$ along that boundary will be known. This also leads to a reduction in unknowns. In addition, the line integrals for both the pressure head and one of its spatial derivatives will be non-zero for the nodes along the boundary.

RESULTS

Some initial results obtained with the Hermitian scheme are given below. The examples are presented as a verification of the accuracy of the numerical scheme, and also to illustrate the type of problems that have been solved thus far.

One-dimensional vertical infiltration

In this example,[12] water is allowed to infiltrate into a deep homogeneous soil profile that has the following hydraulic properties:

$$\theta(h) = \begin{cases} 0.6829 - 0.09524\ln(|h|) & h \leqslant -29.484 \\ 0.4531 - 0.02732\ln(|h|) & -29.484 \leqslant h \leqslant -14.495 \end{cases} \quad (25a)$$

$$K(h) = \begin{cases} 19.34 \times 10^4 |h|^{-3.4095} & h \leqslant -29.484 \\ 516.8\,|h|^{-0.97814} & -29.484 \leqslant h \leqslant -14.495 \end{cases} \quad (25b)$$

where K is given in cm/day and h in cm. The initial moisture content distribution is

$$\theta(x, z, 0) = \begin{cases} 0.15 - z/1200 & -60 \leqslant z \leqslant 0 \\ 0.20 & -125 \leqslant z \leqslant -60 \end{cases} \quad (26)$$

The equivalent initial pressure profile follows immediately from equations (25a) and (26). The medium was divided into 25 rectangular elements ($\Delta x = 10$ cm, $\Delta z = 5$ cm) with a total of 52 nodes. No-flow boundary conditions ($q_n = 0$) were applied at the sides, and a constant pressure head was imposed at the soil surface ($h = -14.495$ cm). A free draining soil profile was assumed at $z = -125$ cm:

$$\frac{\partial h}{\partial z}(x, -125, t) = 0. \quad (27)$$

Figure 3 presents calculated moisture distributions versus depth for four different quadrature schemes. The solid line represents the assumed correct solution and was obtained with several one-dimensional finite difference and finite element solutions that used extremely small time and spatial increments.[8] Relatively poor results were generated with the four-point Gaussian quadrature (2 x 2 GP) scheme. The calculated distributions not only lag behind the correct solution, but also exhibit serious oscillations. Much better results were obtained with the nine-point Gaussian quadrature (3 x 3 GP) scheme, although the computed distributions also in this case lag somewhat behind the correct solution. The most accurate results were obtained with the 16-point Gaussian (4 x 4 GP) and the nine-point alternative (4 + 5 QS) integration schemes. This last scheme actually generated results that were slightly better than those obtained with the 4 x 4 GP scheme. The 4 + 5 QS scheme nearly duplicated the correct solution, except for some minor oscillations near the toe of the moisture front.

Table 1 gives a summary of the various computer runs for this example, including a comparison of the execution times needed to complete the 0.4-day simulation on an IBM 360/91 computer. The table also shows results that were

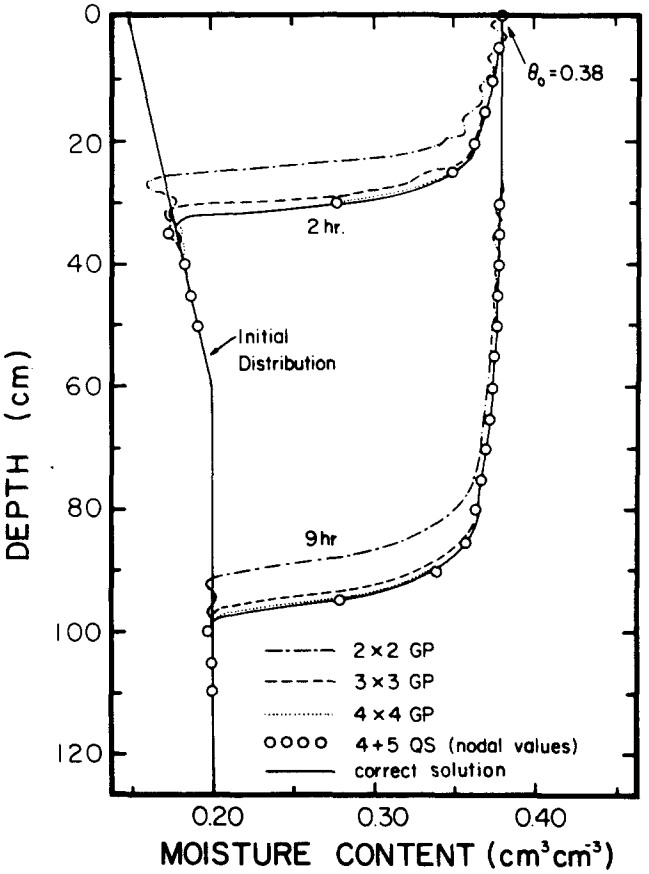

Figure 3. Effect of different quadrature schemes on computed moisture distributions

obtained with equivalent one-dimensional Hermitian finite element solutions.[8] For example, the four-point Gaussian quadrature scheme in two dimensions reduces to a two-point Gaussian scheme (2 GP) in one dimension. Similarly, the 4 + 5 quadrature scheme reduces to (and produces the same results as) a five-point Lobatto integration scheme (5 LP). The infiltration example shows that the 4 + 5 quadrature scheme generates results that are at least as accurate as those obtained with 4 x 4 Gaussian quadrature (Fig. 2), but with a saving in computer time of about 45% (Table 1). The equivalent savings for the one-dimensional programs are considerably less.

Two-dimensional horizontal infiltration

This example considers the two-dimensional horizontal infiltration of water into an initially air-dry, semi-infinite soil slab. A detailed description of the physical problem is given by Rubin.[13] In summary, water infiltrates from the left side of the rectangular soil slab under the influence

Table 1. Summary of various one-dimensional (1-D) and two-dimensional (2-D) simulations of example 1. Total simulation time is 0.4 days

Integration method		Total number of time steps	CPU time (s)	
1-D	2-D	1-D and 2-D	1-D	2-D
2 GP	2 x 2 GP	132	6.6	63.6
3 GP	3 x 3 GP	170	9.9	130.8
4 GP	4 x 4 GP	149	10.2	160.0
5 LP	4 + 5 QS	156	9.4	89.8

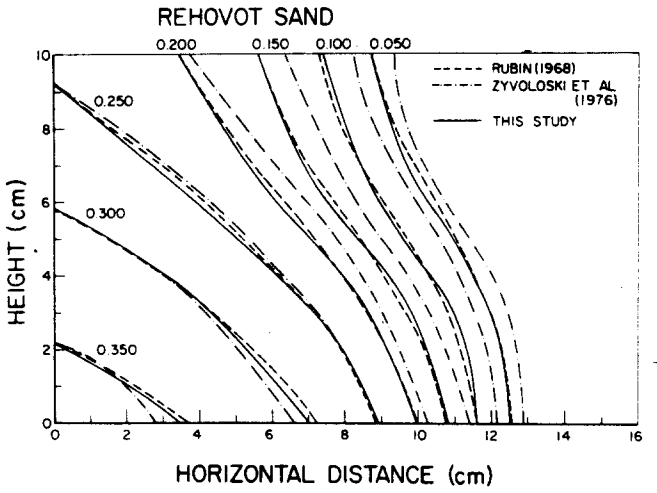

Figure 4. Calculated moisture distributions during infiltration into a horizontal soil slab

of a constant total head ($h+z$) of -13 cm. No-flow boundary conditions are present along the top ($z=0$) and bottom ($z=-10$ cm) boundaries of the system. Soil-hydraulic properties of the Rehovot sand used in the experiment are given elsewhere.[13,14] Figure 4 compares the Hermitian simulation results after 10 min of infiltration with results obtained earlier by Rubin[13] using finite differences and by Zyvoloski *et al.*[15] using linear finite elements. Note that the Hermitian-based moisture distributions are very close to the distributions calculated by Rubin.[13]

Subsurface irrigation

This example describes the infiltration of water from a horizontal line source in a two-dimensional cross-section. Water is applied through buried laterals (point sources) that are located at a depth of 15 cm below the soil surface (Fig. 5). The experiment was used earlier by Thomas *et al.*[16] to compare calculated and measured steady-state pressure head distributions in a soil box designed to model a subsurface irrigation system. The calculated distributions were based on an analytical solution developed by Zachmann and Thomas.[17] This solution holds for a semi-infinite soil medium with no-flow boundary conditions at $x=\pm x_0$. Here we will compare the analytical solution with Hermitian finite element results using exactly the same experimental conditions as described by Thomas *et al.*[16]

Figure 5 shows schematically the finite element mesh for the line source problem. The soil slab was extended arbitrarily to a depth of 350 cm, thereby assuming that the semi-infinite system was closely approximated by this deep profile. The source strength Q equals 1.05×10^{-3} cm^3/cm/s, which is equivalent to a constant application rate of 0.7436 cm/day when distributed evenly over the entire soil surface. The hydraulic conductivity K (cm/day) of the clay loam soil is

$$K = 96.768\exp(-0.1258h) \quad (h \geqslant 0) \qquad (28)$$

Two methods can be used to evaluate the steady-state pressure distribution. One approach would be to calculate the distribution directly by forcing the time-derivative in equation (1) to be zero. This method often requires numerous iterations and could at times even lead to convergence problems, especially for highly non-linear problems. The direct method was followed first. However, several numerical adjustments were required in the program, such as an

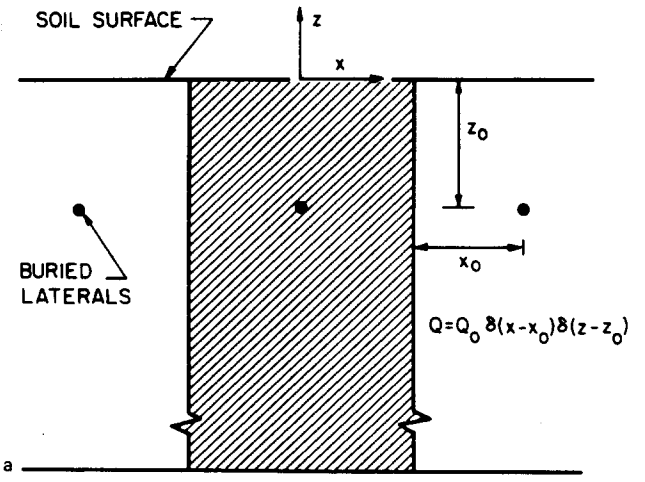

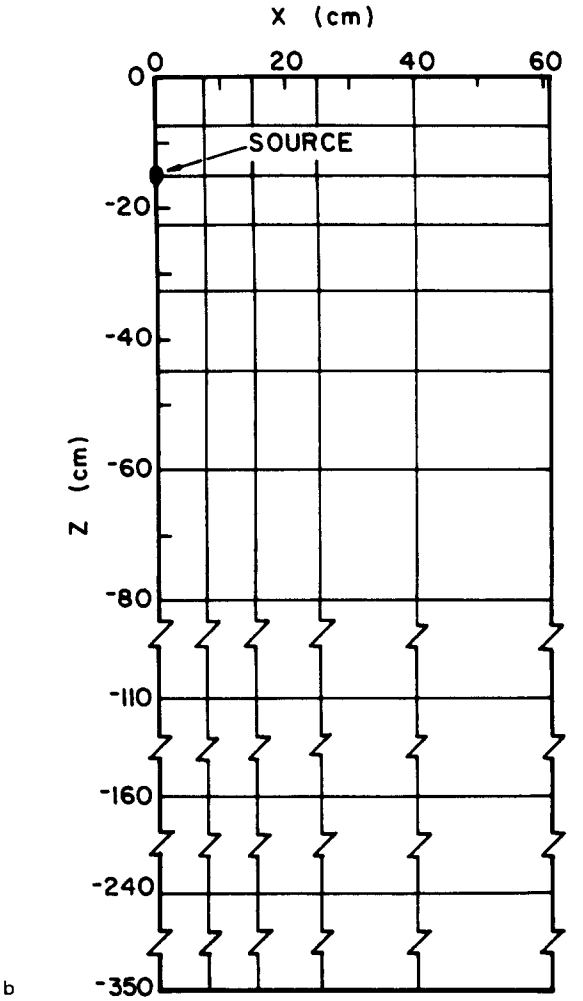

Figure 5. Schematic representation of the line source problem and the associated finite element mesh

effective under-relaxation, to speed up convergence and hence to limit the number of iterations. Alternatively, the problem can be solved indirectly by starting out with an arbitrary initial condition and solving the problem as if it were a transient one. A fictitious soil water retention curve was used for this purpose. This last approach proved to be much easier and less costly.

Calculated steady-state pressure head distributions are shown in Fig. 6. The curves duplicated exactly the analytical results obtained with the solution of Zachmann and Thomas.[17] The pressure head deep in the profile was found

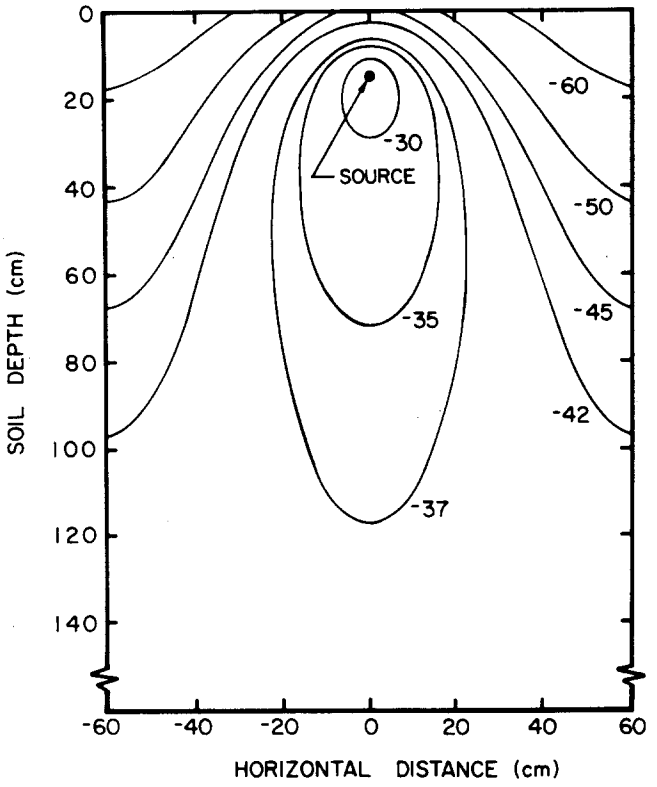

Figure 6. Calculated steady-state pressure head distribution resulting from a buried line source at z = −15 cm (semi-infinite profile)

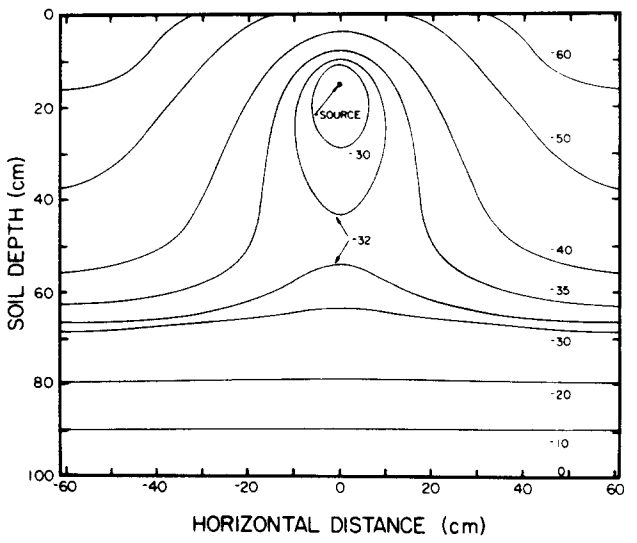

Figure 7. Calculated steady-state pressure head distribution resulting from a line source at z = −15 cm (fixed water table at −100 cm)

to be −38.7 cm, and was independent of the horizontal coordinate. The value of −38.7 cm is consistent with the pressure head at which the hydraulic conductivity reaches a value of 0.7436 cm/day, the latter being the application rate as averaged over the soil surface. As a modification of the last example, Fig. 7 shows calculated steady-state pressure head distributions resulting from the same line source as before, but now with a fixed water table present at $z = -100$ cm. Note that the pressure distributions close to the soil surface are nearly identical to those shown in Fig. 6.

CONCLUSION

The three examples shown in this study demonstrate that the Hermitian finite element solution can be used to calculate pressure head (and moisture content) distributions for a number of two-dimensional problems. Application of the alternative 4 + 5 Lobatto-type quadrature scheme results in considerable computer savings as compared to the use of Gaussian quadrature. Because the Hermitian solution generates a continuous flow velocity field for most finite element configurations, it is expected that the scheme will be especially attractive when combined with numerical solutions of the solute transport equation.

REFERENCES

1 Hanks, R. J. and Bowers, S. A. Numerical solution of the moisture flow equation for infiltration into layered soils, *Soil Sci. Soc. Am. Proc.* 1962, **26**, 530
2 Freeze, R. A. The mechanism of natural groundwater recharge and discharge. 1. One-dimensional, vertical, unsteady, unsaturated flow above a recharging or discharging groundwater flow system, *Water Resources Res.* 1969, **5**, 153
3 Brandt, A., Bresler, E., Diner, N., Ben-Asher, I., Heller, J. and Goldberg, D. Infiltration from a trickle source. I. Mathematical models, *Soil Sci. Soc. Am. Proc.* 1971, **35**, 675
4 Pikul, M. F., Street, R. L. and Remson, I. A numerical model based on coupled one-dimensional Richards and Boussinesq equations, *Water Resources Res.* 1974, **4**, 1069
5 Neuman, S. P. Saturated-unsaturated seepage by finite elements, *J. Hydraulics Div., ASCE* 1973, **99**, HY12:2233-2251
6 Reeves, M. and Duguid, J. O. Water movement through saturated-unsaturated porous media: a finite-element Galerkin model. ORNL-4927, Oak Ridge National Lab., Oak Ridge, Tenn., 1975
7 Segol, G. A three-dimensional Galerkin-finite element model for the analysis of contaminant transport in saturated-unsaturated porous media. In: *Finite Elements in Water Resources*, Gray, W. G., Pinder, G. F. and Brebbia, C. A., eds., Pentech Press, London, pp. 2.123-144, 1977
8 van Genuchten, M. Th. A comparison of numerical solutions of the one-dimensional unsaturated-saturated flow and mass transport equations, *Adv. Water Resources* 1982, **5**, 47
9 van Genuchten, M. Th., Pinder, G. F. and Frind, E. O. Simulation of two-dimensional contaminant transport with isoparametric finite elements, *Water Resources Res.* 1977, **13**, 451
10 Gray, W. G. and van Genuchten, M. Th. Economic alternatives to Gaussian quadrature over isoparametric quadrilaterals, *Int. J. Num. Methods Eng.* 1978, **12**, 1478
11 Frind, E. O. An isoparametric Hermitian element for the solution of field problems, *Int. J. Num. Methods Eng.* 1977, **11**, 945
12 Warrick, A. W., Biggar, J. W. and Nielsen, D. R. Simultaneous solute and water transfer for an unsaturated soil, *Water Resources Res.* 1971, **7**, 1216
13 Rubin, J. Theoretical analysis of two-dimensional transient flow in unsaturated and partly saturated soils, *Soil Sci. Soc. Am. Proc.* 1968, **32**, 607
14 Rubin, J. Numerical analysis of ponded rainfall infiltration. In: *Water in the Unsaturated Zone*, Rijtema, P. E. and Wassink, H., eds., Wageningen, Netherlands, Vol. I, pp. 440-451, 1969
15 Zyvoloski, G., Bruch, J. C., Jr. and Sloss, J. M. Solution of equation for two-dimensional infiltration problems, *Soil Sci.* 1976, **122**, 65
16 Thomas, A. W., Duke, H. R., Zachmann, D. W. and Kruse, E. G. Comparisons of calculated and measured capillary potentials from line sources, *Soil Sci. Soc. Am. J.* 1976, **40**, 10
17 Zachmann, D. W. and Thomas, A. W. A mathematical investigation of steady infiltration from line sources, *Soil Sci. Soc. Am. Proc.* 1973, **37**, 495